

Spatiotemporal intermittency and scaling laws in inhomogeneous coupled map latticesAshutosh Sharma^{1,2} and Neelima Gupte²¹*Department of Physics, University of Pune, Pune 411007, India*²*Department of Physics, Indian Institute of Technology, Madras 600036, India*

(Received 8 February 2002; published 20 September 2002)

We study the phenomenon of intermittency in an inhomogeneous lattice of coupled maps where the inhomogeneity appears in the form of different values of the map parameter at adjacent sites. This system exhibits spatiotemporal intermittency as well as purely spatial intermittency accompanied by temporal periodicity in different regions of the parameter space. Both types of intermittency appear as a result of bifurcations of codimension two in such systems. We identify the types of bifurcations that are seen. The intermittency near the bifurcation points and lines is associated with power-law distributions for the laminar lengths. The scaling laws for the laminar length distributions are obtained. Two distinct types of scaling behavior characterized by power laws with exponents that fall in two distinct ranges can be seen in the neighborhood of codimension-two bifurcation points. Additionally we find two crossover exponents.

DOI: 10.1103/PhysRevE.66.036210

PACS number(s): 05.45.-a

I. INTRODUCTION

The phenomenon of spatiotemporal intermittency has been observed in a wide range of extended systems in the laboratory as well as in a variety of theoretical models. Spatio-temporal intermittent behavior has been seen in theoretical models such as coupled map lattices [1–6], partial differential equations [7,8], as well as in experimental systems such as chemical reactions [9], Rayleigh-Benard convection in narrow channels and annuli [10,11], planar Couette flow [12], studies of fluid flows between rotating eccentric cylinders such as the Taylor-Dean [13] and Taylor-Couette [14,15] flows, and the “printer’s instability” [16]. A variety of scaling laws have been observed in these systems. However, there are no definite conclusions about their universal behavior. Many of the observed phenomena have been seen in experimental systems where no simple model is available. It is therefore important to study spatiotemporal intermittency in simple model systems which are amenable to theoretical and numerical analysis. Again, the conjecture that the transition to spatiotemporal intermittency falls in the same universality class as directed percolation [17] has been the central issue in a long debate in the literature [3,4,18,19]. Model studies can provide important pointers in this debate.

We study the phenomenon of spatiotemporal intermittency in an inhomogeneous lattice of diffusively coupled logistic maps. We shall take our definition of spatiotemporal intermittency to be a region where a fluctuating mixture of regular and turbulent regions is seen and scaling laws indicative of long-range correlations are found in the distribution of laminar lengths. The inhomogeneity appears in the form of different values for the map parameter at distinct sites. Such inhomogeneous lattices have been considered in the case of pinning studies [20] and in the context of control of spatiotemporal chaos [21]. Our model shows spatiotemporal intermittency in the vicinity of bifurcations [22] of codimension one and codimension two.

In the case of bifurcations from the synchronised fixed point, we find the bifurcation curves by local analysis. These

curves intersect at various points in the parameter space indicating the existence of bifurcations of codimension two. Spatiotemporal intermittency is seen in the vicinity of these points. (See Fig. 1 for space-time plots of spatiotemporal intermittency.) A temporally periodic structure with long-range correlations appears in the neighborhood of the codimension-two tangent-period doubling bifurcation which undergoes a further bifurcation to spatiotemporal intermittency [23]. The distribution of laminar lengths seen in the case of both spatial and spatiotemporal intermittency shows power-law behavior. Four distinct types of scaling behavior are seen. Two of the exponents correspond to two distinct types of behavior. In addition, two exponents that appear to be crossover exponents are seen. Exponents similar to those observed by us are seen in several experiments and also in other models.

We define the model in Sec. II, and also carry out linear stability analysis for bifurcations from the synchronised fixed point. The plot of bifurcation lines in parameter space obtained from this analysis provides a good indicator of regions where spatiotemporal intermittency can be found in the parameter space and is discussed in the same section. The distribution of laminar lengths in the intermittent regions follow power-law scaling behavior. This behavior is discussed in Sec. III. Our results and their implications are discussed in Sec. IV.

II. THE MODEL AND LOCAL ANALYSIS

We consider a lattice of coupled logistic maps such that maps at even lattice sites $2i$ have a given value of the map parameter, say μ , and maps at odd lattice sites have a different value of the map parameter, say μ' . Our model is defined by the evolution equations

$$x_{2i}^{t+1} = (1 - \epsilon)f_{\mu}(x_{2i}^t) + \frac{\epsilon}{2}[f_{\mu'}(x_{2i-1}^t) + f_{\mu'}(x_{2i+1}^t)], \quad (1)$$

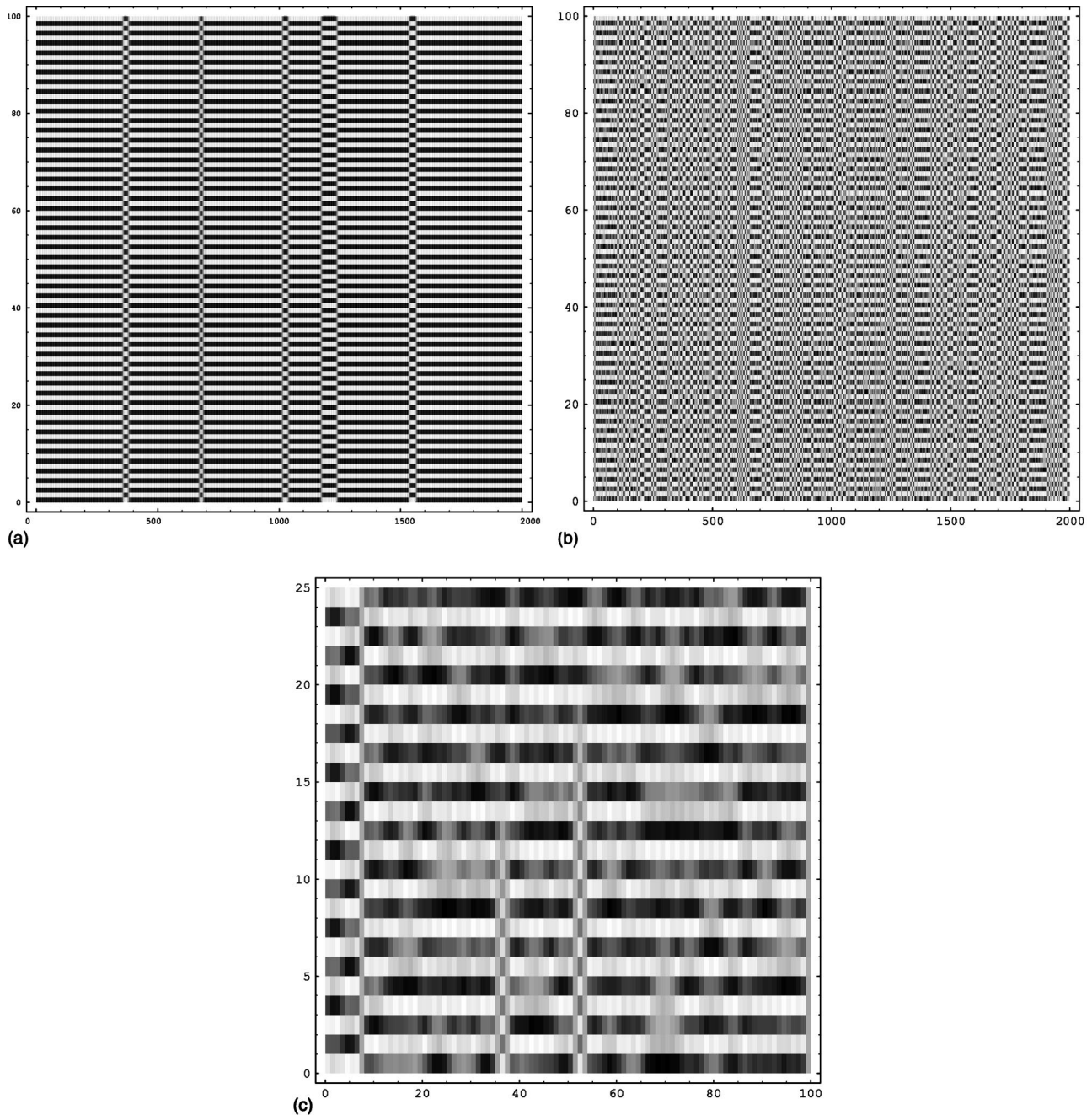


FIG. 1. Space-time plot of a lattice of 2000 sites iterated for 100 iterates at the parameter values $\gamma=1.99$, $\epsilon=0.48$ (i.e., in the neighborhood of the tangent-period-doubling point C). A transient of 20 000 iterates has been discarded. (b) Space-time plot of a lattice of 2000 sites iterated for 100 iterates at the parameter values $\gamma=0.66$, $\epsilon=0.39$ (i.e., in the neighborhood of the tangent-period-doubling point F). A transient of 20 000 iterates has been discarded. (c) Space-time plot of a lattice of 200 sites iterated for 25 iterates at the parameter values $\gamma=0.66$, $\epsilon=0.39$ (i.e., in the neighborhood of the tangent-period-doubling point F). A transient of 5000 iterates has been discarded.

where $f_{\mu}(x)=\mu x(1-x)$ is the logistic map and $\mu, \mu' \in [0,4]$, x_{2i}^t is the value of the variable x at the even lattice site $2i$ at time t , and $0 \leq x \leq 1$. In the case of x_{2i+1}^t , the variable defined at odd lattice sites, the evolution equation is defined by the evolution above with $2i$ being replaced by $2i+1$ and μ and μ' interchanged. We set $\mu' = \mu - \gamma$ and use periodic

boundary conditions with $2N$, the number of lattice sites being even. It can be easily seen that the synchronized fixed points of the system are given by $x^*=0$ and $x^*=(\mu - \gamma\epsilon - 1)/(\mu - \gamma\epsilon)$.

Expanding the evolution equations about the synchronized fixed point, the linear stability matrix has the form

$$J = \begin{bmatrix} (1-\epsilon)f'_\mu(x) & \frac{\epsilon}{2}f'_{\mu'}(x) & 0 & 0 & \dots & 0 & \frac{\epsilon}{2}f'_{\mu'}(x) \\ \frac{\epsilon}{2}f'_{\mu'}(x) & (1-\epsilon)f'_{\mu'}(x) & \frac{\epsilon}{2}f'_{\mu'}(x) & 0 & \dots & 0 & 0 \\ 0 & \frac{\epsilon}{2}f'_{\mu'}(x) & (1-\epsilon)f'_\mu(x) & \frac{\epsilon}{2}f'_{\mu'}(x) & \dots & 0 & 0 \\ 0 & 0 & \frac{\epsilon}{2}f'_{\mu'}(x) & (1-\epsilon)f'_\mu(x) & \dots & 0 & 0 \\ \dots & \dots & \dots & \dots & \dots & \dots & \dots \\ \dots & \dots & \dots & \dots & \dots & \dots & \dots \\ 0 & 0 & \dots & \dots & \dots & (1-\epsilon)f'_\mu(x) & \frac{\epsilon}{2}f'_{\mu'}(x) \\ \frac{\epsilon}{2}f'_{\mu'}(x) & 0 & \dots & \dots & \dots & \frac{\epsilon}{2}f'_{\mu'}(x) & (1-\epsilon)f'_{\mu'}(x) \end{bmatrix}, \quad (2)$$

where $x = x^*$. It is clear that this matrix is of the block circulant form. Therefore, one can carry out similarity transformations by which it can be put in a block diagonal form [24,25]. This similarity transformation can be achieved by the matrix $F_{2N} = F_N \otimes I_2$. Here F_N is a Fourier matrix of size $N \times N$ [26] and I_2 is an identity matrix of size 2×2 . The block diagonal form is given by

$$J' = \begin{pmatrix} M(\theta_1) & 0 & 0 & \dots & 0 \\ 0 & M(\theta_2) & 0 & 0 & \dots \\ \vdots & \vdots & \vdots & \vdots & \vdots \\ \vdots & \vdots & M(\theta_l) & \vdots & \vdots \\ \vdots & \vdots & \vdots & \vdots & \vdots \\ 0 & 0 & 0 & M(\theta_{N-1}) & 0 \\ 0 & 0 & 0 & 0 & M(\theta_N) \end{pmatrix}, \quad (3)$$

where each block, $M(\theta_l)$ is a 2×2 matrix of the form

$$M(\theta_l) = \begin{bmatrix} (1-\epsilon)f'_\mu(x) & \frac{\epsilon}{2}(1+e^{i\theta_l})f'_{\mu'}(x) \\ \frac{\epsilon}{2}(1+e^{-i\theta_l})f'_{\mu'}(x) & (1-\epsilon)f'_{\mu'}(x) \end{bmatrix}, \quad (4)$$

where, $\theta_l = [2\pi(l-1)]/N$, $l = 1, \dots, N$.

The eigenvalues of this matrix as a function of θ_l are given by

$$\lambda(\theta_l) = \frac{(1-\epsilon)(f'_\mu + f'_{\mu'}) \pm \{(1-\epsilon)^2(f'_\mu - f'_{\mu'})^2 + 2\epsilon^2(f'_\mu f'_{\mu'})[1 + \cos(\theta_l)]\}^{1/2}}{2}. \quad (5)$$

Since the eigenvalues of the system lie between $\lambda(0)$ and $\lambda(\pi)$ [25] the bifurcations from the two synchronized fixed points can be obtained by looking at the conditions at which these eigenvalues cross the unit circle. If we fix $\mu = 4$, these conditions define a set of curves in the two parameter ϵ - γ space. Codimension-one bifurcations can take place at parameter values along these curves. These curves intersect in several places where the equations are simultaneously satisfied. At these intersections two eigendirections become unstable, resulting in bifurcations of codimension two.

Thus, we need to consider the eigenvalues

$$\lambda_{\pm}(0) = \frac{(1-\epsilon)(f'_\mu + f'_{\mu'}) \pm [(1-\epsilon)^2(f'_\mu - f'_{\mu'})^2 + 4\epsilon^2(f'_\mu f'_{\mu'})]^{1/2}}{2} \quad (6)$$

TABLE I. We list the equations of the bifurcation lines plotted in Fig. 1 for bifurcations from the synchronized solutions in the ϵ - γ parameter space. We list the label of the bifurcation line, the equation of the bifurcation curve, the type of bifurcation that takes place, and the fixed point from which the solution bifurcates in the table. Here $x_1^* = 0$ and $x_2^* = (\mu - \gamma\epsilon - 1)/(\mu - \gamma\epsilon)$. The abbreviation PD refers to a period-doubling bifurcation.

Line number	Equation of line	Type	Fixed point
1	$\epsilon = \frac{5\gamma - 25}{9\gamma - 40}$	PD	x_1^*
2	$\epsilon = \frac{3 - \gamma}{4 - \gamma}$	Tangent	x_1^*
3	$\epsilon = \frac{3}{4}$	Tangent	x_1^*
4	$\epsilon = \frac{3\gamma - 9}{7\gamma - 24}$	Tangent	x_1^*
5	$\epsilon = \frac{-(8 - \gamma^2 + \gamma)}{2\gamma(\gamma - 4)} + \frac{[(8 - \gamma^2 + \gamma)^2 - 8\gamma(\gamma - 2)(\gamma - 4)]^{1/2}}{2\gamma(\gamma - 4)}$	PD	x_2^*
6	$\epsilon = \frac{(3\gamma + 8) - [(3\gamma + 8)^2 - 64\gamma]^{1/2}}{8\gamma}$	PD	x_2^*
7	$\frac{\gamma\epsilon - 2}{4 - \gamma\epsilon} = \frac{[(1 - \epsilon)(8 - \gamma) + \{(1 - \epsilon)^2(8 - \gamma)^2 - 4(1 - 2\epsilon)(16 - 4\gamma)\}^{1/2}]}{2(1 - 2\epsilon)(16 - 4\gamma)}$	Tangent	x_2^*
8	$\frac{\gamma\epsilon - 2}{4 - \gamma\epsilon} = \frac{[(1 - \epsilon)(8 - \gamma) - \{(1 - \epsilon)^2(8 - \gamma)^2 - 4(1 - 2\epsilon)(16 - 4\gamma)\}^{1/2}]}{2(1 - 2\epsilon)(16 - 4\gamma)}$	Tangent	x_2^*
9	$\frac{\gamma\epsilon - 2}{4 - \gamma\epsilon} = \frac{[-(1 - \epsilon)(8 - \gamma) + \{(1 - \epsilon)^2(8 - \gamma)^2 - 4(1 - 2\epsilon)(16 - 4\gamma)\}^{1/2}]}{2(1 - 2\epsilon)(16 - 4\gamma)}$	PD	x_2^*
10	$\frac{\gamma\epsilon - 2}{4 - \gamma\epsilon} = \frac{[-(1 - \epsilon)(8 - \gamma) - \{(1 - \epsilon)^2(8 - \gamma)^2 - 4(1 - 2\epsilon)(16 - 4\gamma)\}^{1/2}]}{2(1 - 2\epsilon)(16 - 4\gamma)}$	PD	x_2^*

and

$$\lambda_{\pm}(\pi) = \frac{(1 - \epsilon)(f'_{\mu} + f'_{\mu'}) \pm (1 - \epsilon)(f'_{\mu} - f'_{\mu'})}{2}, \quad (7)$$

where $f'_{\mu} = f'_{\mu}(x^*) = \mu(1 - 2x^*)$, and x^* is the synchronized fixed point. Consider the parameter regime $\mu = 4$, $0 \leq \epsilon \leq 1$, $0 \leq \gamma \leq 4$. All the eigenvalues are real in this parameter regime and cross the unit circle on the real axis at ± 1 leading to tangent and period-doubling bifurcations [27]. The equations for the bifurcation curves in the ϵ - γ space obtained by imposing these bifurcation conditions are listed in Table I.

A rich variety of spatiotemporal behavior can be seen in the neighborhood of the bifurcation curves. We concentrate on regions that exhibit spatiotemporal intermittency where a fluctuating mixture of regular and irregular domains can be seen. Spatiotemporally intermittent solutions are possible at many places in the parameter space, particularly in the neighborhood of the bifurcation curves and the vicinity of the

codimension-two points as can be seen from Table II. In addition to the phenomenon of spatiotemporal intermittency seen near these points, the inhomogeneous lattice has regions in parameter space where pure spatial intermittency accompanied by temporally periodic behavior can be seen, i.e., the temporal behavior is periodic, but spatially laminar and turbulent regions co-exist at any point in time. This phenomenon has been discussed elsewhere [23].

We plot the bifurcation curves for bifurcations from the synchronized fixed points in the ϵ - γ space where $0 \leq \epsilon \leq 1$ and $0 \leq \gamma \leq 4$ in Fig. 2. The table indicates the type of bifurcation that takes place along each curve. Since $\mu = 4$ all the eigenvalues are real and tangent and period doubling bifurcations are seen where the eigenvalues cross the unit circle along the real axis. The bifurcation curve 1 is a period-doubling bifurcation from the fixed point $x^* = 0.0$ and the curves 2, 3, and 4 are tangent bifurcation curves from the same fixed point. Curves 5, 6, 9, and 10 are period-doubling bifurcations from the other fixed point $x^* = (\mu - \gamma\epsilon - 1)/(\mu - \gamma\epsilon)$, whereas curves 7 and 8 are tangent bifurca-

TABLE II. We list the codimension-two points where bifurcation lines from the synchronized fixed points intersect. Label 1 corresponds to a bifurcation from the fixed point $x_1^*=0$ and label 2 to those from the fixed point $x_2^*=(\mu-\gamma\epsilon-1)/(\mu-\gamma\epsilon)$. The type of bifurcation involved and the manner in which the eigenvalue crosses unit circle and the power-law exponent $P(l)\approx l^{\zeta_i}$ are listed. The parameter values listed are the values at which the spatiotemporal intermittency with the listed exponent is seen. This point is in the neighborhood of the codimension-two point of column one. The range of the exponent ζ_1 is 1.9–2.2, ζ_2 lies in the range 1.5–1.75, and ζ_3 in the range 0.9–1.15. We also identify the nature of the intermittency, whether spatial or spatiotemporal (ST). We note that the spatial intermittency near point E (see *) is a mixture of temporal periods.

Codimension-two points	Exponent	Parameter region	Eigenvalue	Type	Nature
A	ζ_1	$\gamma=1.18, \epsilon=0.63$	1, -1	T1-PD1	Spatial
B		$\gamma=1.6, \epsilon=0.66$	-1, -1	PD1-PD2	Transient
C	ζ_1	$\gamma=1.99, \epsilon=0.48$	1, -1	T1-PD2	Spatial
D	ζ_1	$\gamma=2.6, \epsilon=0.969$	+1, -1	T2-PD2	Spatial
E	ζ_1	$\gamma=2.5, \epsilon=.35$	1, -1	T1-PD2	Spatial*
F	ζ_F	$\gamma=0.66, \epsilon=0.39$	1, -1	T1-PD2	STI

tions from this point. These bifurcation lines intersect at various points in the parameter space indicating the existence of codimension two bifurcations. Spatiotemporal intermittency is seen in the neighborhood of several of these codimension-two points. These are indicated by the letters A–F in Fig. 2. We note that points A and D are points which lie on the intersection of tangent and period-doubling lines 2 and 1 where $x^*=0.0$ goes unstable and lines 8 and 10 where the fixed point $x^*=(\mu-\gamma\epsilon-1)/(\mu-\gamma\epsilon)$ goes unstable. These two points show the phenomenon of pure spatial intermittency which has been discussed in detail elsewhere [23]. The point B where the two period doubling lines 1 and 9 corresponding, respectively, to the points $x^*=0.0$ and $x^*=(\mu-\gamma\epsilon-1)/(\mu-\gamma\epsilon)$ intersect is a period-doubling, period-doubling point. The spatiotemporal intermittency seen here is a transient phenomenon. The tangent line 2 from the fixed point $x^*=0$ intersects with the period-doubling line 9 from $x^*=(\mu-\gamma\epsilon-1)/(\mu-\gamma\epsilon)$ at the codimension point C whereas it intersects with the line 6 from the same fixed point at the codimension-two point E. Lines 4 and 5, which

correspond to a tangent bifurcation from $x^*=0.0$ and a period-doubling bifurcation from $x^*=(\mu-\gamma\epsilon-1)/(\mu-\gamma\epsilon)$ intersect at point F. The space-time plots of the spatiotemporal behavior at points C and F can be seen in Figs. 1(a)–1(c). We note that all the codimension-two points where spatiotemporal intermittency is seen are tangent-period-doubling points, as the phenomenon near the period-doubling-period-doubling point B disappears after a transient.

The space-time plot of Fig. 1(c) (i.e., point F) looks quite different from the space time plots seen in Fig. 1(a). We also note that there are several codimension-two points where no spatiotemporal intermittency is seen in the neighborhood. Notably, the intersections of line 3 with other lines show no spatiotemporal intermittency and intersections that correspond to γ values greater than 3 do not show any intermittent behavior in their neighborhood.

The plot of bifurcation curves in parameter space provides a good indicator of the regions where spatiotemporal intermittency can be seen. However, bifurcations from higher period solutions can give rise to further structure in this parameter space and regions where spatiotemporal intermittency can be seen may be more extensive than that predicted by this phase diagram.

III. SCALING LAWS FOR SPATIOTEMPORAL INTERMITTENCY

The behavior of the distribution of laminar lengths is an important statistical characterizer of spatiotemporal intermittency [4,3]. The length of the laminar bursts, i.e., the number of consecutive sites that follow periodic behavior before being interrupted by chaotic bursts is calculated. The distribution for this length shows a power-law behavior with $P(l)\approx l^{-\zeta}$, where $P(l)$ is the probability for a laminar length of size l (see Figs. 3 and 4). This shows the presence of long-range spatial correlations in the lattice.

We observe that power-law scaling is seen in extensive regions of the parameter space. Four distinct types of scaling behavior were seen in the parameter space. We plot $\ln P(l)$

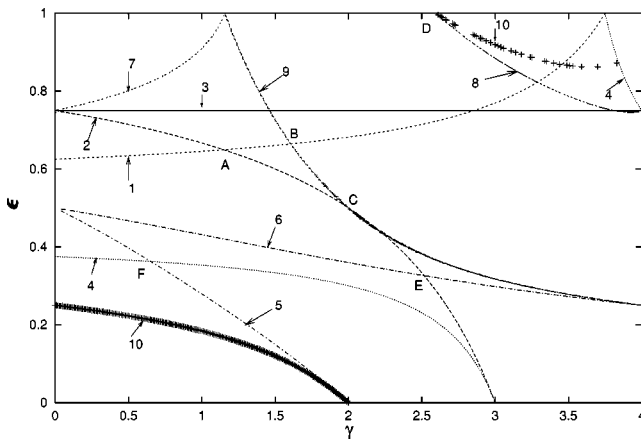


FIG. 2. We plot the bifurcation lines in parameter space for bifurcations from the two fixed points $x^*=0$ and $x^*=(\mu-\gamma\epsilon-1)/(\mu-\gamma\epsilon)$ for $0.01\leq\gamma\leq 4.0$, $0\leq\epsilon\leq 1$. The equations of the bifurcation lines can be found in Table I.

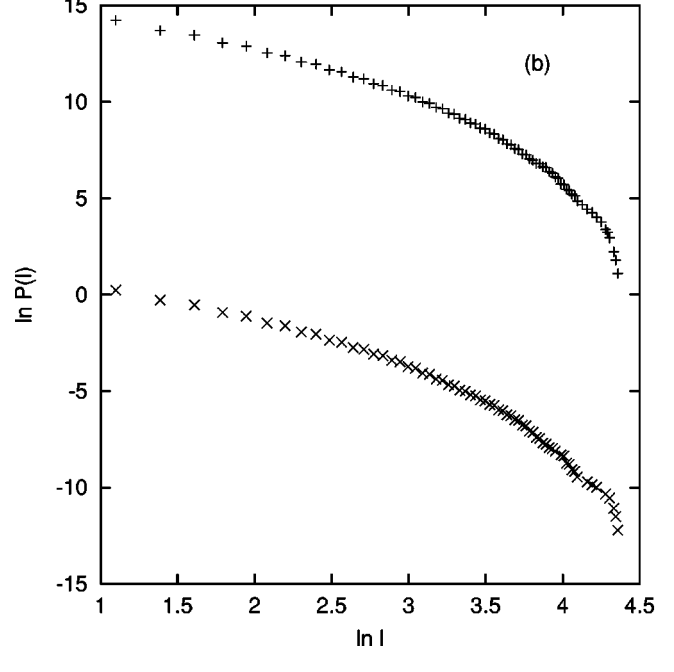
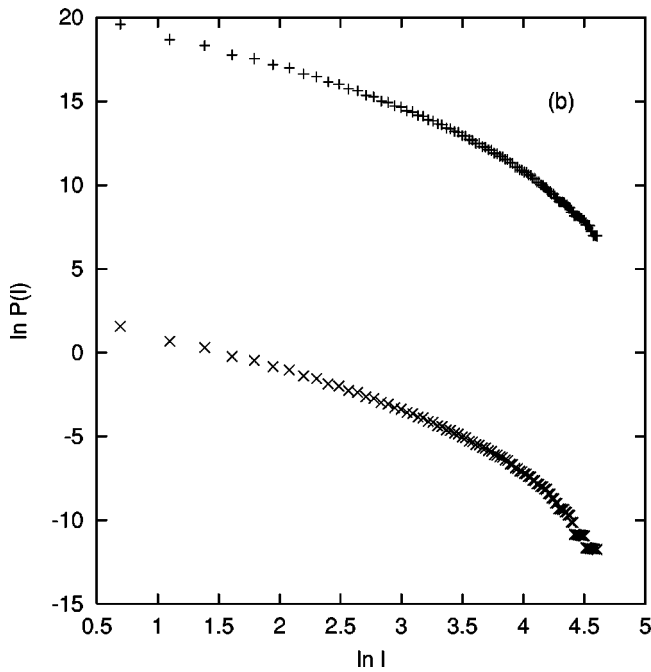
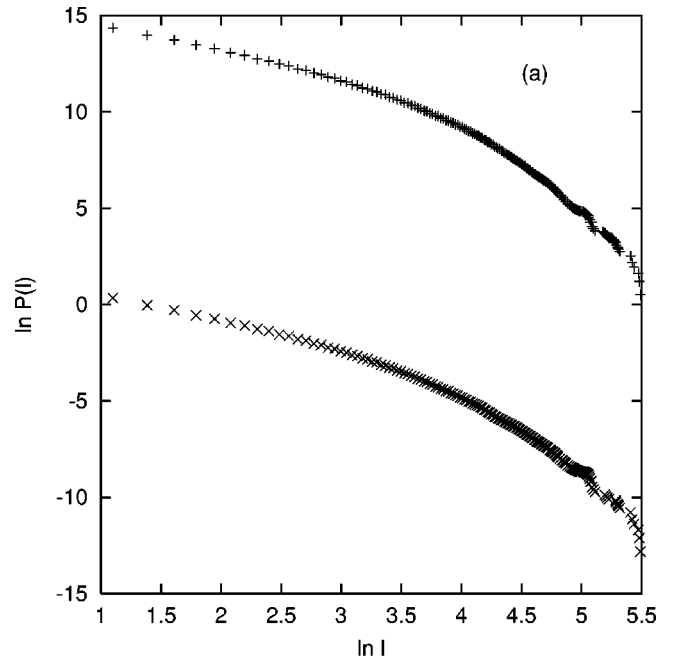
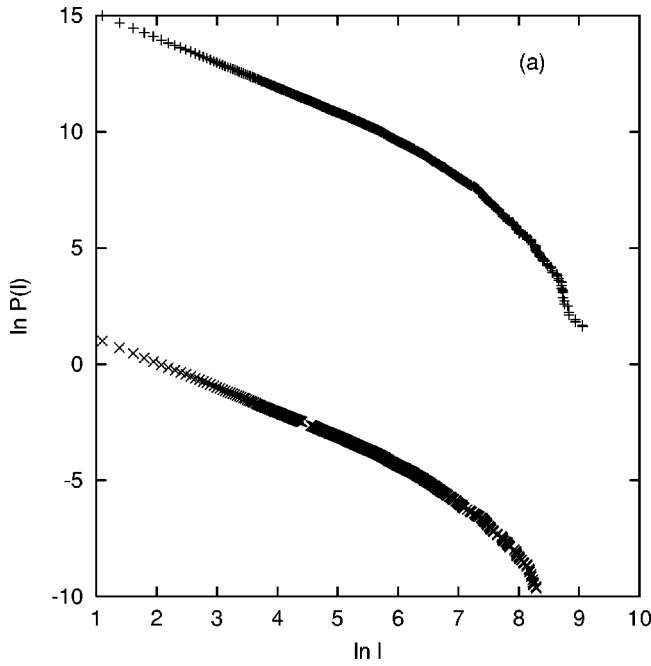


FIG. 3. (a) shows the plot of $\ln P(l)$ vs $\ln l$ at the parameter values $\gamma=1.99$, $\epsilon=0.48$ for 10 000 lattice sites (plus signs) and 5000 lattice sites (crosses), each iterated for 100 000 iterates. An initial transient of 5000 iterates has been discarded. A straight line of slope -1.1 can be fitted to the data. An average over 25 random initial conditions has been taken. The laminar lengths l are in units of lattice spacing here and in all subsequent graphs. (b) shows $\ln P(l)$ vs $\ln l$ at the parameter values $\gamma=0.66$, $\epsilon=0.39$ for 10 000 lattice sites (plus signs) and for 5000 lattice sites (asterisks) each iterated for 100 000 iterates for ten initial conditions. An initial transient of 10 000 iterates has been discarded. A straight line of slope -2.0 can be fitted to the data up to the third decade.

FIG. 4. (a) shows a plot of $\ln P(l)$ vs $\ln l$ at the parameter values $\gamma=1.0$, $\epsilon=0.64$ for 10 000 lattice sites (plus signs) and 5000 lattice sites (crosses) each iterated for 100 000 iterates for 25 initial conditions. An initial transient of 10 000 iterates has been discarded. A straight line of slope -1.33 can be fitted to the data up to the third decade. (b) shows $\ln P(l)$ vs $\ln l$ at the parameter values $\gamma=1.0$, $\epsilon=0.425$ for 10 000 lattice sites (plus signs) and for 5000 lattice sites (crosses) each iterated for 100 000 iterates for 25 initial conditions. An initial transient of 10 000 iterates has been discarded. A straight line of slope -1.66 can be fitted to the initial part of the data.

against $\ln l$ for four typical values in the parameter space in Figs. 3(a) and 3(b) and 4(a) and 4(b). It is clear that four distinct exponents can be seen. Each figure shows plots of $\ln P(l)$ versus $\ln l$ for a distinct parameter value, for two lattice sizes 5000 and 10 000 as indicated in the figure captions. (A constant value has been added to the data of lattice size 10 000 to shift it upwards.) We find that a good fit to the data is obtained for the values $\zeta_1=1.1$, $\zeta_2=1.33$, $\zeta_3=1.66$, and $\zeta_F=2.0$. The power laws ζ_1 and ζ_F can be seen in Figs. 3(a) and 3(b), whereas power laws ζ_2 and ζ_3 are seen in Figs. 4(a) and 4(b). We note that the power laws ζ_F , ζ_2 , and ζ_3 are only seen up to the third or fourth decade and the distribution falls off faster than a power law thereafter, whereas the power law ζ_1 maintains its behavior over a much longer stretch.

An indication of the regions where power laws are seen can be obtained by looking at the bifurcation lines where the synchronized fixed points become unstable as plotted in Fig. 2 and in the neighborhood of their intersection points. We observe four distinct ranges for the exponents. These are ζ_1 which lies between 0.9 and 1.15, ζ_2 which takes values between 1.2 and 1.35, ζ_3 which lies between 1.5 and 1.75, and ζ_F which takes values between 1.9 and 2.2.

It is clear from Fig. 3(a) that the $P(l)$ for the exponent ζ_1 shows power-law behavior over a range of l values from 1 to a few hundred lattice sites whereas the $P(l)$ for the exponent ζ_F [Fig. 3(b)] exhibits power-law behavior over l values ranging from 1 to a few decades. The difference between the two types of behavior can also be seen in the space-time plots of Fig. 1. It is interesting to note that the power law ζ_1 is seen in the neighborhood of the codimension-two points $A-E$ whereas the exponent ζ_F is seen in the neighborhood of the codimension-two point F . As can be seen from the space-time plots, the laminarity for the power law ζ_1 can be checked to very high accuracy, and has been checked to an accuracy of 10^{-5} for these plots. However, the laminarity in the neighborhood of the power law ζ_F is checked to the value 10^{-1} due to the presence of large variations that can again be seen on the space-time plots. Thus the spatial correlations are far stronger in the vicinity of the ζ_1 points than in the vicinity of the ζ_F points.

A similar phenomenon is seen even in the case of the exponents shown in Fig. 4. In the case of Fig. 4(a), the ζ_2 exponent is a sustained power law over a somewhat larger range of l values than the power law ζ_3 seen in Fig. 4(b). We note that the scaling exponents ζ_2 and ζ_3 can be regarded as cross-over exponents as the behavior crosses over from power-law to exponential behavior. The exponent ζ_2 is seen along line 2 where there are many codimension-two intersections so that the scaling behavior is ζ_1 in the neighborhood of the tangent-period-doubling points along the curve, moves away from ζ_1 to the value ζ_2 , and comes back to ζ_1 as the next codimension-two point is encountered. However, the value ζ_3 is encountered along line 6 when the scaling behavior moves away from ζ_1 to exponential fall off. We show the exponential fall off in Figs. 5(a) and 5(b). Figure 5(a) is a plot of $P(l)$ against l and Fig. 5(b) plots $\ln P(l)$ against l . The behavior seen can be fitted by the exponential function (dot-

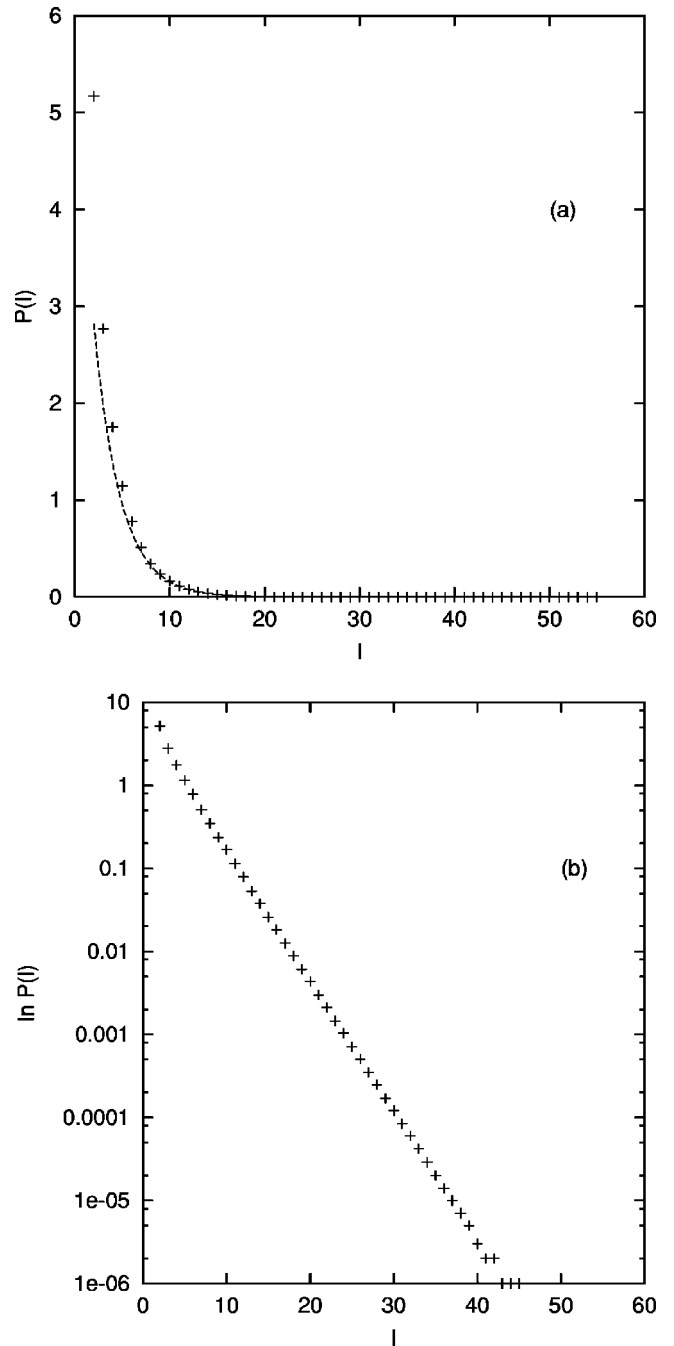


FIG. 5. (a) shows the plot of $P(l)$ vs l at the parameter values $\gamma=0.25$, $\epsilon=0.45$ for 10 000 lattice sites iterated for 100 000 iterates for five initial conditions. The function fitted is $f(x) = 5.8 \exp(-0.36x)$. (b) shows the plot of $\ln P(l)$ vs l for the same data.

ted line) given in the figure caption. Since the exponents ζ_2 and ζ_3 are crossover exponents, it is unsurprising that the power law is sustained over just a few decades. Again, the exponent ζ_3 , which is the exponent for cross-over to exponential behavior, shows power-law behavior over a shorter range of l -s than ζ_2 which shows sustained power-law behavior over a slightly larger range of l values due to its proximity to bifurcation points where ζ_1 behavior, which corresponds to stronger spatial correlations, is seen. We also

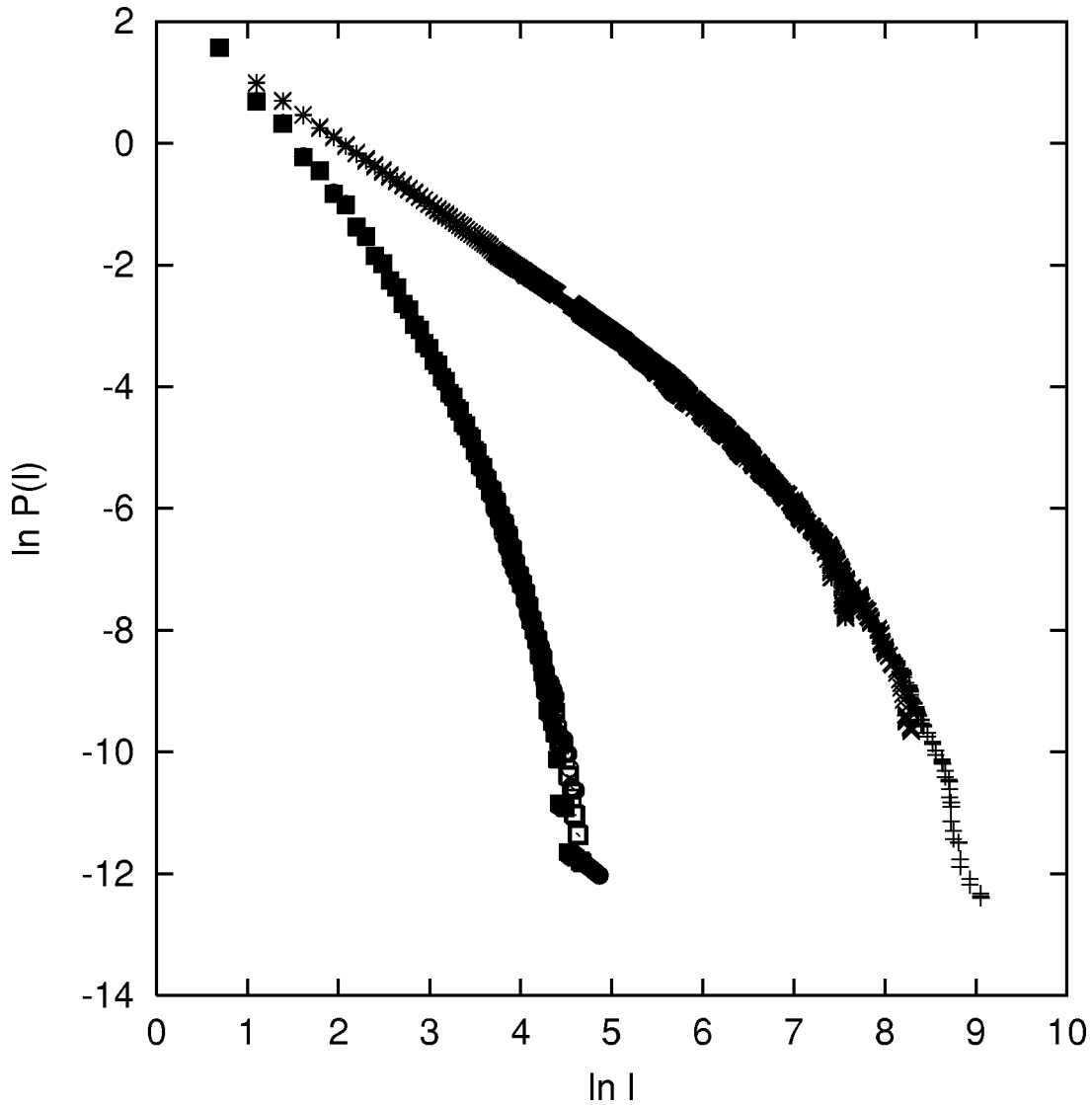


FIG. 6. Plots of $\ln P(l)$ vs $\ln l$ at two parameter values. The upper set (which corresponds to the power law ζ_1) is for the parameters $\gamma=1.99$, $\epsilon=0.48$ for 10 000 lattice sites (plus signs), 5000 lattice sites (crosses), and 2000 lattice sites (asterisks). Each lattice has been iterated for 100 000 iterates after discarding 10 000 iterates for 25 initial conditions. The lower set (those for the power law ζ_F) is for the parameter values $\gamma=0.66$, $\epsilon=0.39$ for 10 000 lattice sites (circles), 5000 lattice sites (hollow boxes), and 2000 lattice sites (filled boxes). Each lattice has been iterated for 100 000 iterates after discarding 10 000 iterates for ten initial conditions.

note that while the exponents ζ_2 and ζ_3 appear to indicate crossover behavior, they still fall in distinct ranges. No sustained spatiotemporal intermittency is seen along other lines.

The phenomena discussed above have been observed for lattices of different sizes. We show the power law ζ_1 for three different lattice sizes (10 000 lattice sites, 5000 lattice sites, and 2000 lattice sites) in Fig. 6. It is clear that data for different lattice sizes fall on the same curve. The longest laminar lengths seen are of the order of 10% of the lattice size so that finite size effects are not seen. Even in the cases of the scaling law ζ_F , where the power-law behavior is seen over a much shorter range of l values, the data for different sizes of lattice fall on the same curve as can be seen in Fig. 6. Figure 7 shows the power laws ζ_1 for 50 000 and 100 000 iterates and ζ_F for 100 000 and 150 000 iterates for a lattice of 10 000 sites. The power law is the same in the linear parts

of the curves. All the results above are obtained for bifurcations from the synchronized fixed points. Bifurcations from higher spatial temporal periods can also give rise to spatiotemporal or spatial/temporal intermittency in many additional regions of parameter space. This question is presently under investigation.

IV. DISCUSSION AND CONCLUSIONS

We have shown that both spatial and spatiotemporal intermittency can arise in an inhomogeneous coupled map lattice. The phenomenon of intermittency is more widespread in inhomogeneous lattices than in the case of homogeneous lattices. The presence of pure spatial intermittency accompanied by temporally periodic behavior is an unusual feature that arises in the case of the inhomogeneous system under

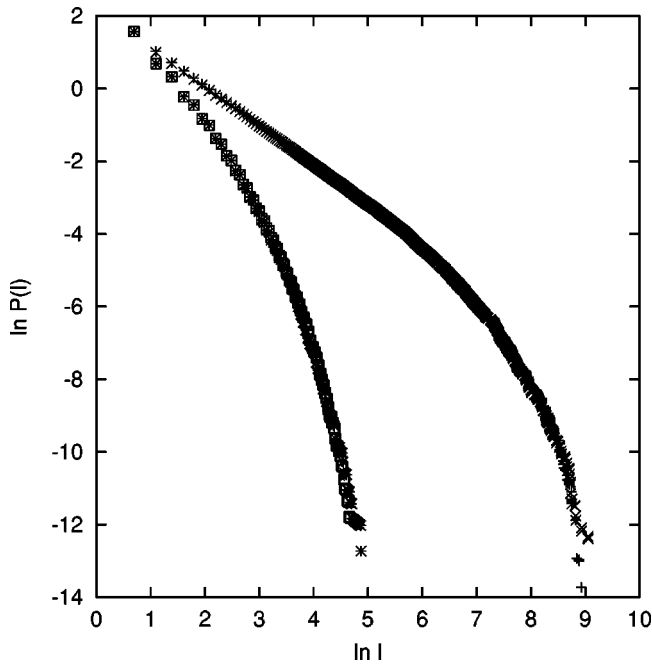


FIG. 7. Plot of $\ln P(l)$ vs $\ln l$ at the parameter values $\gamma=1.99$, $\epsilon=0.48$ for 10 000 lattice sites, 50 000 iterates (plus signs) and 100 000 iterates (crosses) for 25 initial conditions each. The plot also shows $\ln P(l)$ vs $\ln l$ at the parameter values $\gamma=0.66$, $\epsilon=0.39$ for 10 000 lattice sites, 100 000 iterates (boxes) and for 150 000 iterates (asterisks) for ten initial conditions. An initial transient of 10 000 iterates has been discarded.

study [23]. The intermittency arises as a result of bifurcations of codimension one and two. Such bifurcations are also of interest in the case of other spatially extended systems [28].

The distributions of laminar lengths seen exhibit four distinct kinds of power-law scaling behavior characterized by exponents which fall in four distinct ranges. It is interesting

to note that exponents similar to those observed by us have been seen in quasi-one-dimensional fluid experiments. An exponent that falls in the same range as our exponent ζ_F has been observed in the case of Rayleigh-Benard convection in an annulus [11], whereas exponents that fall in the same range as ζ_2 have been seen for convection in a channel and for the Taylor-Dean experiment [14,13]. It would also be interesting to see if exponents similar to ours are seen in the case of fluid systems with inhomogeneities. A situation in which there is a regular array of inhomogeneities as in our model could be one where an array of heating elements maintained at a desired profile of temperatures is introduced in a fluid. The inhomogeneity could also be in the form of obstacles to the fluid flow or the existence of a vortex lattice.

The plot of bifurcation curves in parameter space for bifurcations from synchronized fixed point solutions forms a rough phase diagram which indicates regions where spatiotemporal intermittency can be found. Spatiotemporal intermittency can be found in the vicinity of the bifurcation curves and in the vicinity of the intersections of these curves. Secondary bifurcations and bifurcations from higher period solutions can provide further structure to this phase diagram. The analogy of the transition to spatiotemporal intermittency with second-order phase transitions is being explored further.

The conjecture that the transition to spatiotemporal intermittency falls in the same universality class as directed percolation [17] has been the central issue in a long debate in the literature [4,3,18,19]. Much work on coupled map lattices has shown that this conjecture is very hard to verify due to the presence of long-range correlations. Our model could be useful for comparisons of the critical behavior of spatiotemporal intermittency with those of directed percolation and in discussions of universality properties. We hope our analysis will be useful for the understanding of intermittent phenomena arising in other spatially extended systems as well, and in discussions of their genericity and universality.

-
- [1] *Theory and Applications of Coupled Map Lattices*, edited by K. Kaneko (Wiley, 1993), and references therein.
 - [2] K. Kaneko, Prog. Theor. Phys. **58**, 112 (1987); Physica D **34**, 1 (1989).
 - [3] J. Rolf, T. Bohr, and M.H. Jensen, Phys. Rev. E **57**, R2503 (1998).
 - [4] H. Chate and P. Manneville, Physica D **32**, 409 (1988).
 - [5] C.I. Christov and G. Nicolis, Physica A **228**, 326 (1996).
 - [6] *Dynamical Systems Approach to Turbulence*, edited by T. Bohr, M.H. Jensen, G. Paladin, and A. Vulpiani (Cambridge University Press, Cambridge, 1998).
 - [7] H. Chate, Nonlinearity **7**, 185 (1994).
 - [8] M.G. Zimmermann, R. Toral, O. Piro, and M. San Miguel, Phys. Rev. Lett. **85**, 3612 (2000).
 - [9] R. Kapral, in *Theory and Applications of Coupled Map Lattices*, (Ref. [1]), Chap. 5, p. 135.
 - [10] F. Daviaud, M. Dubois, and P. Berge, Europhys. Lett. **9**, 441 (1989).
 - [11] S. Ciliberto and P. Bigazzi, Phys. Rev. Lett. **60**, 286 (1988).
 - [12] S. Bottin, F. Daviaud, O. Dauchot, and P. Manneville, Europhys. Lett. **43**, 171 (1998).
 - [13] M.M. Degen, I. Mutabazi, and C.D. Andereck, Phys. Rev. E **53**, 3495 (1996).
 - [14] G. Colovas and C. David Andereck, Phys. Rev. E **55**, 2736 (1997).
 - [15] A. Goharzadeh and I. Mutabazi, Eur. Phys. J. B **19**, 157 (2001).
 - [16] S. Michalland, M. Rabaud, and Y. Couder, Europhys. Lett. **22**, 17 (1993).
 - [17] Y. Pomeau, Physica D **23**, 3 (1986).
 - [18] J.M. Houlrik, I. Webman, and M.H. Jensen, Phys. Rev. A **41**, 4210 (1990).
 - [19] P. Grassberger and T. Schreiber, Physica D **50**, 177 (1991).
 - [20] R.O. Grigoriev, M.C. Cross, and H.G. Schuster, Phys. Rev. Lett. **79**, 2795 (1997).
 - [21] Q. Zhilin and Hu Gang, Phys. Rev. E **49**, 1099 (1994).
 - [22] J. Guckenheimer and P. Holmes, *Nonlinear Oscillations, Dy-*

- namical Systems and Bifurcations of Vector Fields* (Springer-Verlag, New York, 1983), Chap. 3, p. 117.
- [23] A. Sharma and N. Gupte, *Int. J. Bifurcation Chaos* **12**, 1363 (2002).
- [24] P.J. Davis, *Circulant Matrices* (Wiley, New York, 1973).
- [25] P.M. Gade and R.E. Amritkar, *Phys. Rev. E* **47**, 143 (1993).
- [26] A Fourier matrix F_k (where k denotes the dimension of the matrix) is defined as $F_k^*(i,j) = (1/\sqrt{k})(\omega_k^{(i-1)(j-1)})$, where F_k is the conjugate transpose of F_k^* and $\omega_k = e^{2\pi i/k}$.
- [27] If μ is fixed at values less than 4.0, Hopf bifurcations can be seen. Power law scaling is associated with these bifurcations as well. This will be discussed elsewhere.
- [28] G. Iooss, *Turbulence and the Navier-Stokes Equation* (Springer-Verlag, New York, 1989), Vol. 564, pp. 69–84.